Collagen Fibre Orientation and Dispersion Govern Ultimate Tensile Strength, Stiffness and the Fatigue Performance of Bovine Pericardium

A. Whelan[1, 2, 3], J. Duffy[1, 2], R.T. Gaul[1, 2], D. O'Reilly[3], D.R. Nolan[1, 2], P. Gunning[4], C. Lally[1, 2, 5], B. Murphy[1, 2, 5]

[1] Trinity Centre for Bioengineering, Trinity Biomedical Sciences Institute, Trinity College Dublin, Dublin 2, Ireland
[2] Department of Mechanical and Manufacturing Engineering, School of Engineering, Trinity College Dublin, Dublin 2, Ireland
[3] Structural Heart Division, Boston Scientific Corporation, Galway, Ireland
[4]Structural Heart Division, Boston Scientific Corporation, Los Gatos, CA 95032, USA
[5]Advanced Materials and Bioengineering Research Centre (AMBER), Trinity College Dublin, Dublin 2, Ireland

Abstract

The durability of bovine pericardium leaflets employed in bioprosthetic heart valves (BHVs) can significantly limit the longevity of heart valve prostheses. Collagen fibres are the dominant load bearing component of bovine pericardium, however fibre architecture within leaflet geometries is not explicitly controlled in the manufacture of commercial devices. Thus, the purpose of this study was to ascertain the influence of pre-determined collagen fibre orientation and dispersion on the mechanical performance of bovine pericardium.

Three tissue groups were tested in uniaxial tension: cross-fibre tissue (XD); highly dispersed fibre-orientations (HD); or preferred-fibre tissue (PD). Both the XD and PD tissue were tested under cyclic loading at 1.5 Hz and a stress range of 2.7 MPa.

The results of the static tensile experiments illustrated that collagen fibre orientation and degree of alignment significantly influenced the material's response. Whereby, there was a statistically significant decrease in material properties between the XD groups and both the PD and HD groups for ultimate tensile strength and stiffness ($p<0.01$). Furthermore, HD tissue had a stiffness of approximately 58% of the PD group, and XD tissue had a stiffness of approximately 18% of the PD group. The dynamic behaviour of the XD and PD groups was extremely distinct; for example a Weibull analysis indicated that the 50% probability of failure in specimens with fibres orientated perpendicular (XD) to the loading direction occurred at 375 cycles. Due to this failure, XD specimens survived less than 20% of the cycles completed by those in which fibres were aligned along the loading direction (PD).

The results from this study indicate that fibre architecture is a significant factor in determining static strength and fatigue life in bovine pericardium, and thus must be incorporated in the design process to improve future device durability.

1. Introduction

Heart valve disease effects approximately 8% of the population over the age of 65 in the United States [1]. This implies that approximately 5.5 million citizens in the US are currently living with some form of heart valve disease. The primary corrective healthcare focus in this patient cohort is replacement or repair surgery, or minimally invasive intervention. Mitral valve disease is associated with a number of disease forms and heterogeneous corrective measures [2], while aortic valve disease is more homogenous. Aortic valve stenosis (AS) is the predominant manifestation of this, with estimates that outcomes can be fatal in as many as 50% of such patients, two years following the onset of symptoms without intervention [3].

To enhance heart valve disease patient outcomes, two types of valve replacement devices have been developed: mechanical and bioprosthetic heart valves (BHVs). BHVs consist of a structural frame and 'tissue' leaflets; to mimic native leaflets. Currently, BHVs are employed in the majority of replacement procedures, with use in 64% of procedures in 2001 increasing to 82% in 2011 [4]**.** Mechanical valves may also be used to replace a diseased patient's valve, however, the patient is required to take life-long anti-coagulation therapy following device implantation [5]**.** The loading imposed on valve leaflets during each cardiac cycle can be described by three dominant regimes; flexure (opening), shear (blood efflux), flexure again (closing) and finally tension (leaflet coaptation) [6]. Additionally, it is estimated that during systole, stresses in particular regions of the leaflet can reach up to 3.17 MPa, with peak stresses of 1.17 MPa observed in the diastolic phase [7]. BHVs are prone to early failure, with data in the literature clearly indicating that the durability of these devices has not yet been optimised [8]–[12]. Furthermore, it has been reported that the animal

pericardial tissue used to construct the leaflets is a factor/cause of premature BHV failure [13]–[15].

Pericardium is a collagenous tissue which surrounds the heart, and is harvested for leaflet manufacture. Prior to valve mounting, the pericardial tissue is sterilised and fixed with glutaraldehyde. There have been a number of published studies on the mechanical characterisation of this tissue, however results differ greatly between authors [16]. Furthermore, there is limited knowledge of the mechanical fatigue performance of glutaraldehyde fixed bovine pericardium (GLBP) and the mechanical properties of GLBP have been previously investigated only in specific orientations of highly aligned specimens; exclusive of fibre dispersion. Furthermore, these studies were not conducted on commercial tissue specimens, but rather tissue fixed 'in-house' for 1-7 days, and stored in saline thereafter [17]–[22].

Collagen fibres are the dominant load bearing component within pericardial tissue, and as with all fibrous materials, the orientation of the fibres with respect to the direction of loading is an important factor in determining the strength of the material [23]. However, to the authors' knowledge, the native pericardial fibre orientation is not explicitly considered in the manufacture or mounting of GLBP leaflets on current commercial devices. Collagen fibre architecture can be characterised non-destructively with an optical technique, such as small angle light scattering (SALS). SALS analysis has been used in a number of previous studies to quantify collagen fibre orientation and dispersion in bovine pericardium, prior to mechanical testing [17], [22], [24]–[27]. Fibre orientation describes the dominant orientation of fibres within a specimen, i.e. the angle at which fibres are orientated with respect to the loading direction. Fibre dispersion describes how highly dispersed fibres are about this

dominant orientation. High fibre dispersion indicates there are fibres orientated at multiple angles about the dominant orientation, and low dispersion indicates the majority of fibres are aligned along this dominant direction.

The aim of this study was to determine the uniaxial static and dynamic mechanical properties of GLBP, controlling for fibre orientation and dispersion. Potentially, this new knowledge will aid in increasing the durability of future BHV devices.

2. Materials & Methods

2.1. Sample Preparation

GLBP patches were obtained from Neovasc Inc. (British Colombia, Canada), which had been both fixed and stored in 0.5% glutaraldehyde. Dogbone-shape specimens were cut from the patches of tissue with a custom-made die, where the resulting specimen gauge length/width ratio was 5.5:1 (gauge length =12.5 mm and width=2.27 mm). The dogbone specimens were imaged with SALS to ascertain fibre orientation and dispersion (see Section 2.2) and then categorised according to these parameters.

2.2. Small Angle Light Scattering (SALS)

Small angle light scattering (SALS) is a non-destructive, optical technique which utilises scattered light distributions from an incident beam to determine fibre orientation and dispersion in a fibrous sample. The design and development of the specific experimental set-up employed in this study has been previously reported [28]**.** Briefly, the system consists of a helium-neon laser, which passes through a sample held in a motorised positioner. When the incident beam has moved through the sample, the scattered light distribution is projected onto a screen, and an image of the light is captured (see Figure 1). The images are processed in a custom Matlab code (The

MathWorks, Inc., Natick, Massachusetts, United States), which analyses the elliptical scattered light distribution to calculate the dominant fibre angle and the degree of fibre dispersion at each location. According to single-slit diffraction theory [29], light scatters perpendicular to the fibres at each location, and thus the major axis of the elliptical distribution allows for determination of the dominant fibre orientation**.**

The degree of fibre dispersion is presented as an eccentricity value, which is calculated by means of the major and minor axes of the elliptical light at each region of interest [30]. Samples with fibres orientated in multiple directions, at each region of interest, are characterised by a circular ellipse (due to a low minor-to-major axis ratio) and hence a low eccentricity value. Conversely, highly aligned samples exhibit a very dominant major axis, and a high eccentricity value (see Figure 2).

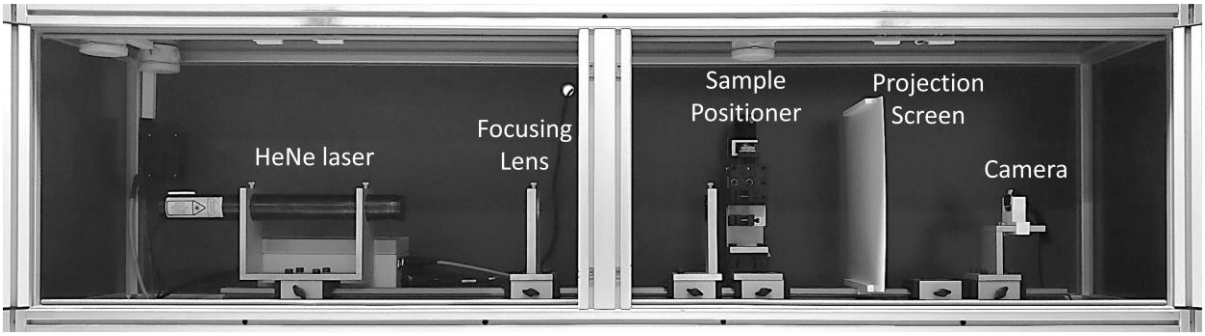

Figure 1: *SALS system; composed of HeNe laser, focusing lens, sample positioner, projection screen and camera [28].*

As the dogbone specimens fail at the centre of the gauge length, a 1 x 3 mm area centred at this location was chosen as the interrogation region. A series of images were taken across this area, at 250µm increments, resulting in a total of 48 images for analysis per sample. Each sample was characterised as preferred fibre (PD), where the dominant fibre orientation is parallel to the direction of loading (0° ± 35°), or cross fibre (XD), where the fibre orientation is aligned perpendicular to the direction of loading (90° ± 35°). Specimens were only categorised as PD or XD if they were highly aligned in these respective directions, i.e. an eccentricity value equal to or above 0.65.

Finally, an additional specimen category was established; highly dispersed (HD), where fibres are orientated in multiple directions (illustrated through an eccentricity value < 0.65) (see Figure 2).

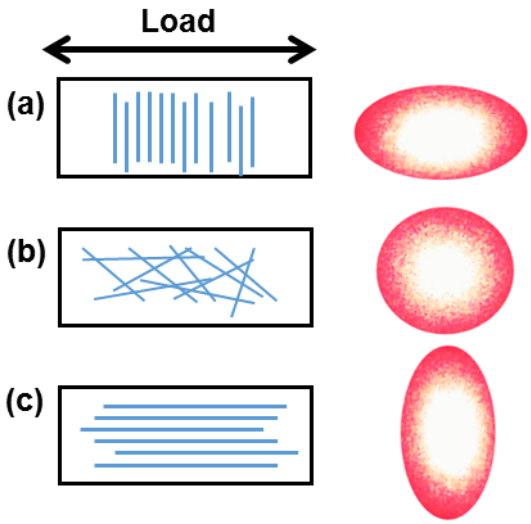

Figure 2: *Schematic illustrating specimen fibre orientation and resulting scattered light ellipse. (a) Cross-fibre specimen (XD), (b) Highly dispersed specimen (HD) and (c) Preferred-fibre specimen (PD).*

2.3. Uniaxial Monotonic Tensile Loading

Dogbone specimens were uniaxially loaded to failure in a Zwick Twin Colum Universal Testing Machine (Zwick Roell Group, Ulm, Germany), where the sample size for each of the three groups (XD, HD, PD) was six ($n=6$). Each specimen was tested at room temperature, and hydrated at the beginning of the test with phosphate buffered saline (Dulbecco's PBS, Sigma Aldrich, D8537). Firstly, the specimen was preconditioned for 5 cycles, between 0.1 MPa and 1 MPa, at 20 mm/minute, and then loaded to failure at 20mm/minute. The test end criterion was defined as the point when the load returns below 80% the maximum force reached. Stiffness (E) was calculated as the slope of the final linear region of the stress-strain curve.

2.4. Uniaxial Cyclic Tensile Loading

Dogbone specimens were uniaxially cyclically loaded in a stress-controlled environment, with a Tytron^{TM} Microforce Testing System (MTS Systems Corporation, MN, USA). Specimens were preconditioned for 1 cycle at 0.01Hz (peak stress 3 MPa), and then repeatedly cycled at 1.5 Hz at a peak stress of 3 MPa, with an R-ratio of 0.1; resulting in a $\Delta\sigma$ of 2.7 MPa (*n=12*). Peak/trough forces and displacements were analysed to measure specimen stiffness, which was calculated as the slope of the stress-strain curve. The test end point was defined as either failure or run-out, at 1 million cycles. Testing was conducted in a water-bath at 37° C, to simulate the physiological environment.

2.5. Statistical Analysis

Values are presented as mean ± standard deviation in this study. Statistical analysis was performed with Prism 6 statistical software (GraphPad Software Inc., San Diego, California). For the monotonic experimental data, a one-way analysis of variance (ANOVA) was performed on the ultimate tensile strength, stiffness and failure strain values to investigate statistical significance between each of the three specimen groups (XD, HD, PD). A Tukey's multiple comparisons test was conducted if the ANOVA test result was statistically significant (i.e. $p<0.05$ for 95% Confidence Interval).

For analysis of fatigue data, a Student's t-test proved insufficient as it assumes a normal distribution of data. As such, a Mann-Whitney unpaired two-tailed t-test was chosen for significance of $p < 0.05$. Additionally, a nonparametric Kaplan-Meier statistical method with a log-rank Mantel-Cox test was chosen for survival analysis. A Weibull probability of failure plot was constructed using Minitab® Statistical Software,

with a confidence interval of 95%. Stiffness data was analysed using a one-way ANOVA with a Bonferroni post-hoc test with confidence interval of 95%. Significance between two groups were analysed using an unpaired t-test for $p < 0.05$.

3. Results

3.1. SALS Analysis

Visual representative contour plots for each specimen category are shown in Figure 3, where the white and black vectors illustrate the fibre orientation at each location across the interrogation region. Each sample category contained six specimens ($n=6$) which met the fibre orientation classification criteria, as described in Section 2.2, the results of this analysis are presented in Table 1 and 2, Appendix A (monotonic and cyclic specimens, respectively).

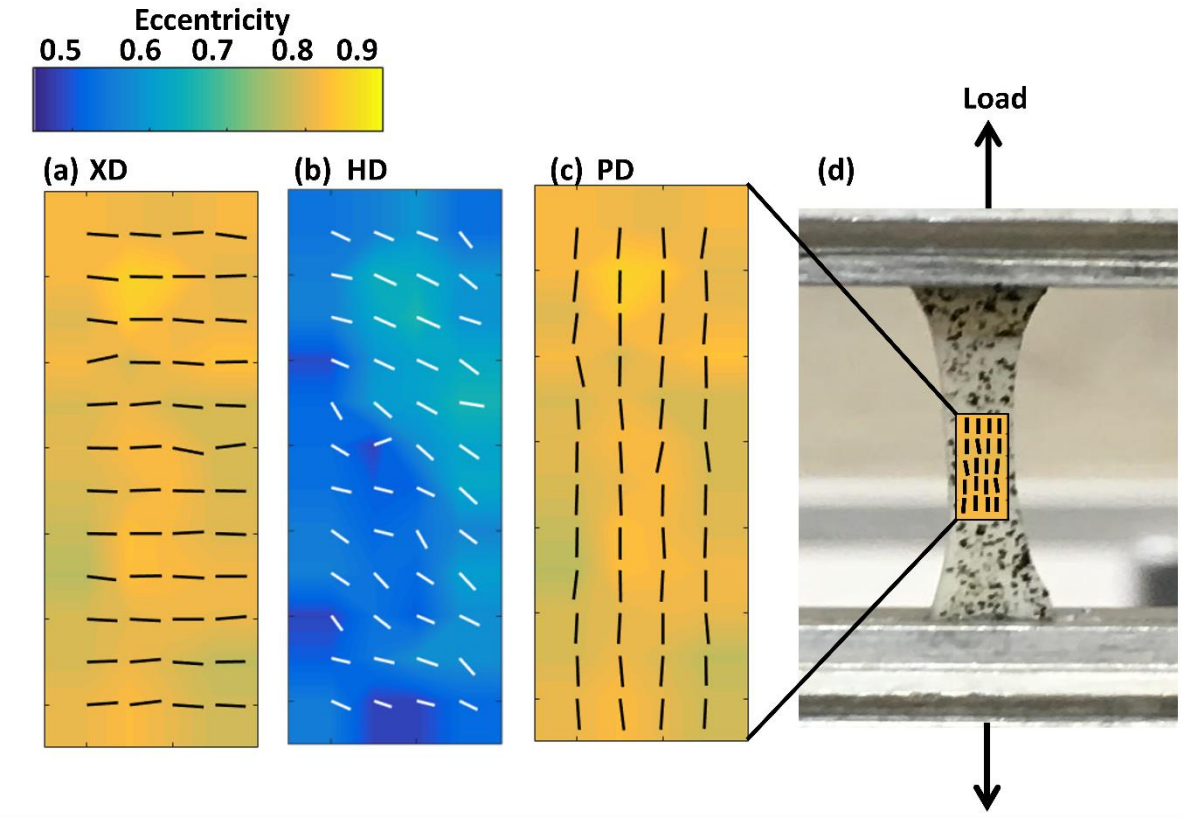

Figure 3: *SALS contour plots for (a) XD, (b) HD and (c) PD specimen groups. (d) SALS Interrogation region of dog-bone specimens prior to tensile loading (Interrogation region measures 1 x 3 mm).*

3.2. Uniaxial Monotonic Mechanical Tests

The summary data for these experiments is presented in figures 4 and 5. It was noted that the ultimate tensile strength (UTS) and stiffness of the PD and HD groups (*UTS*=16.3 ± 6.10 MPa and *E*=144.9 ± 32.32 MPa, 12.63 ± 4.21 MPa and *E*=84.19 ± 13.33 MPa respectively) were statistically significantly greater than that of the XD group (*UTS*=3.90 ± 3.14 MPa and *E*=26.19 ± 21.67 MPa). However, the HD group was not statistically significantly less than the PD group in its ultimate load bearing capacity. The specimen variation within and between groups is illustrated both through the stress-strain plots (see Figure 4) and the high standard deviations associated with each mean UTS value (see Figure 5).

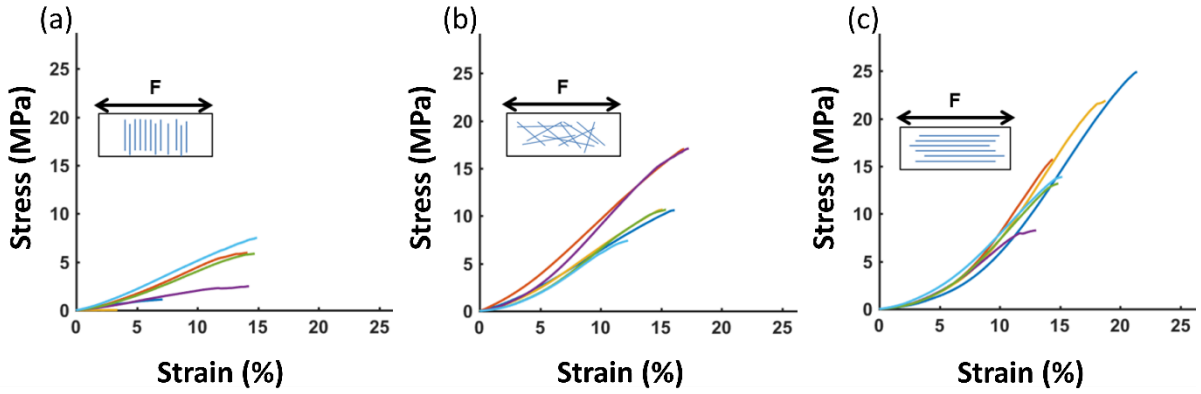

Figure 4: *Stress-Strain curves for uniaxial tensile loading to failure. (a) XD group (b) HD group and (c) PD group.*

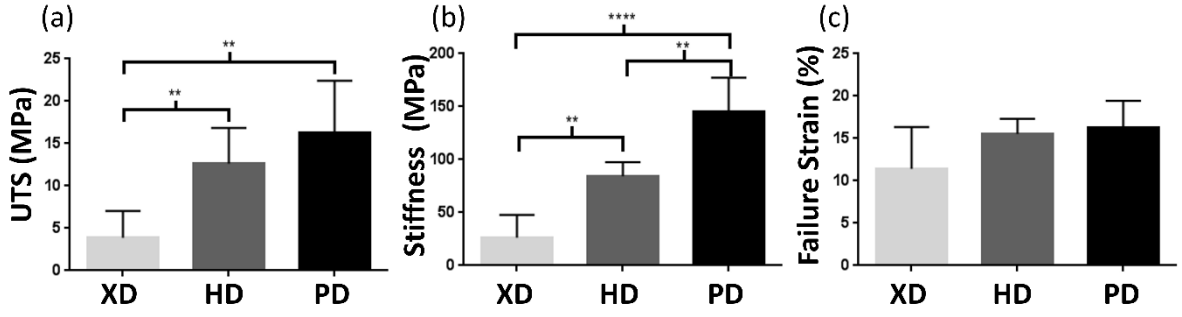

Figure 5: *(a) UTS , (b) Stiffness values (c) Failure strains for each specimen group. *p= <0.05, **p= <0.01, ***p=<0.001 and ****p= <0.0001*

3.3. Uniaxial Cyclic Tensile Loading

XD and PD groups were assessed under uniaxial cyclic loading and the main results are presented in Figure 6. Each PD specimen reached ‘run-out’; which was defined as 1 million cycles. In contrast, the XD specimens failed at significantly lower cycle numbers, where the average was 174,266 ± 369,653 cycles; which is approximately 20% of the PD run-out tests. This group notably exhibited a very high variability, in contrast to the consistent behaviour observed in the PD group. It is important to note that the XD sample with the lowest eccentricity value reached run-out (0.65, see sample ‘XD 6’, Table 2, Appendix A). Analysis of the initial and final loading cycles revealed that each PD specimen increased in stiffness, while XD specimen stiffness either decreased or remained unchanged following loading. The stiffness changes between groups were statistically significant (*p < 0.0001).*

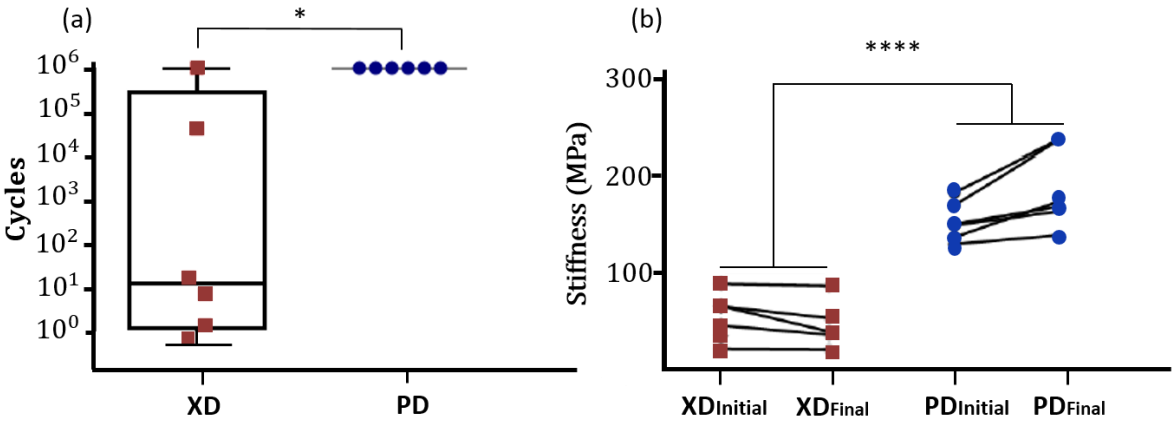

Figure 6: *(a) Cyclic loading results for XD and PD specimen groups p*= <0.05 (b) Change in specimen stiffness for XD and PD specimens p****=< 0.0001*

The Weibull plot for this data-set indicated that although there was no trend towards failure with increasing cycle number for the PD group, the probability of failure did increase for the XD group for increasing cycle number (see Figure 7). This 95% confidence interval plot shows a 50% probability of failure for the XD group at 375 cycles.

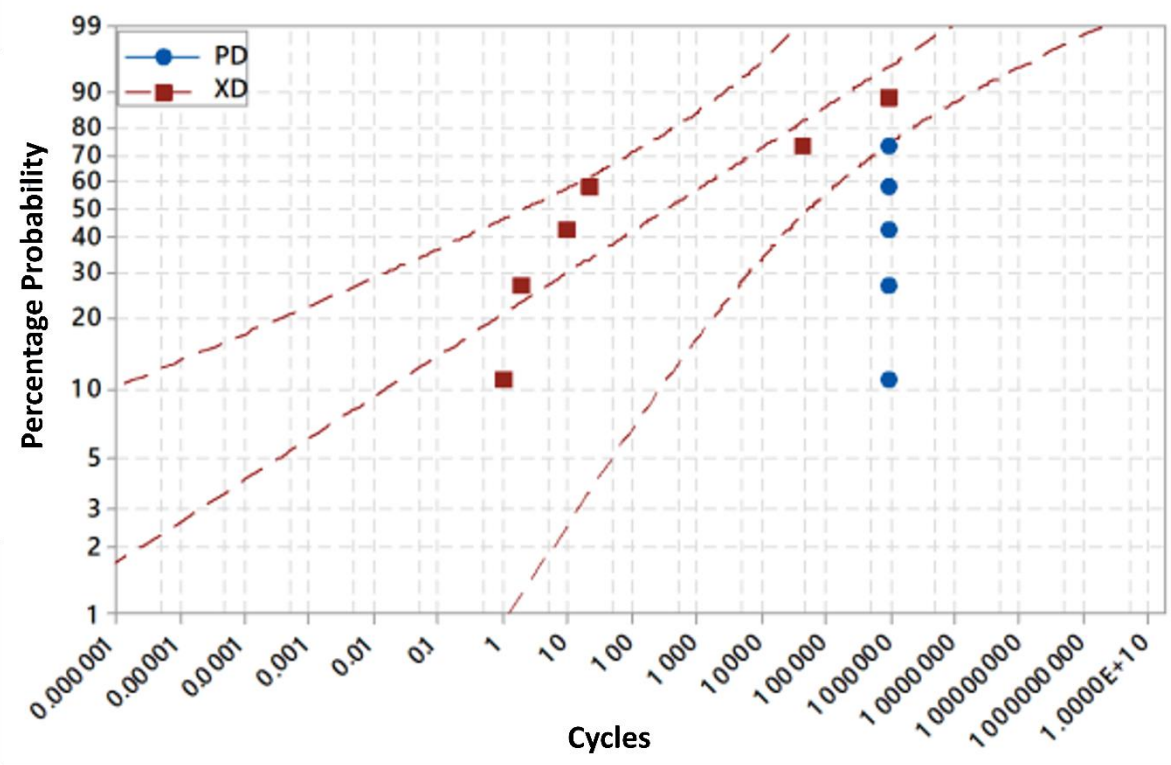

Figure 7: *Weibull plot showing trend towards a higher probability of failure with increasing cycle number for the XD specimens and no trend towards failure for PD specimens.*

4. Discussion

The results presented in this study illustrate the role collagen fibre orientation and dispersion play in the mechanical response of GLBP. SALS analysis allowed for a non-destructive determination of the underlying fibre architecture of specimens prior to testing, which aided in the understanding of the subsequent performance of specimen groupings under differing loading environments.

Statistically significant differences were observed in the mean UTS and stiffness values in the XD group compared to the two remaining groups i.e. the XD values were significantly lower (see Figure 5(a), (b)). Moreover, the high standard deviations associated with all groups were also reflected in the varied stress-strain curves observed in Figure 4. For example, the UTS values recorded for the PD group range from 8.3 MPa to 21.8 MPa. Furthermore, each specimen in the PD group exhibited a non-linear response to loading, typical of collagenous tissues, where the upturn and transition along the curve represents the incremental recruitment of collagen [31]. In contrast, the XD group displayed a more linear loading response; possibly indicating an absence of collagen fibre reorientation, culminating in inadequate collagen recruitment and ultimately, a comparably low load bearing capacity (see Figure 4(a), (c)).

Interestingly, the HD group displayed mechanical properties comparable to that of the PD group, with no statistically significant differences between their respective UTS and failure strains (see Figure 5 (a), (b)). This was noteworthy, as HD specimens are characterised by fibres orientated in multiple directions, as opposed to PD specimens where fibres are predominantly aligned along the loading direction, as in PD samples. Additionally, HD specimens exhibited a minor degree of non-linearity in their response

to loading (see Figure 4 (b)). Characterised by fibres orientated in multiple directions, the nonlinear response to loading seen in the HD group is possibly explained by an adequate proportion of fibres orientated along the loading direction, the stretching and recruitment of which resulted in a load bearing capacity similar to that of the PD group.

Although not statistically significant, it is evident in Figure 5 (c) that the mean failure strain of the XD group was lower than that of the remaining two groups. This was possibly explained by the absence of fibre recruitment during loading, resulting in increased stress in the matrix, leading to tissue-level failure at a lower strain. The failure strain of the PD and HD groups were very similar (16.3 ± 2.7 % and 15.5 ± 1.6 %, respectively), and the macro-failure in such samples is likely due to rupture of previously recruited collagen fibres, as illustrated through the non-linear response to loading (see Figure 4 (b), (c)).

Cyclic testing of PD and XD groups revealed the significant influence of fibre orientation on the fatigue life of specimens. As evident in Figure 6(a), all PD specimens reached run-out, while the XD fatigue life was much lower in comparison. Four samples in this group had failed by 23 loading cycles (see Table 2, Appendix A). Interestingly, an inverse trend was observed for this group between eccentricity and cycles to failure, where the sample with the highest eccentricity value failed after a single loading cycle, in contrast to the sample with the lowest eccentricity value, which was the only XD sample to reach run-out (see sample ‘XD 1’ and ‘XD 6’ respectively, Table 2, Appendix A). Even with this particular specimen’s high number of cycles to failure, the mean behaviour of PD and XD groups was statistically significantly different; culminating in a 50% probability of failure for XD samples at 375 loading cycles (see Figure 7). It is also important to note that PD specimens displayed an

increase in stiffness at the test end point, which is likely due to fibres becoming even more aligned with the loading direction as the cycle number increased (see Figure 6 (b)). The contrast in repeatability of the fatigue life between XD/PD groups further indicates the importance of characterising leaflet fibre orientations, so that fibres can be aligned with principal loading directions *in-vivo.* To investigate this further in future studies, the eccentricity threshold could be increased in order to more explicitly categorise specimens as highly aligned PD/XD (i.e. from 0.65 to 0.75). Furthermore, the fibre orientation range for which specimens are classified as PD/XD could also be narrowed (i.e. 0° ± 15° and 90° ± 15°, respectively).

To the authors' knowledge, previous studies investigating the mechanical properties of GLBP have not explored specimens in which the collagen fibres are highly dispersed [32]–[39]. The noteworthy mechanical strength of the HD group seen in this study warrants further investigation; principally motivated by their multi-fibre orientation. It is hypothesised that BHV leaflets harvested from such regions on the pericardial sac may be particularly well suited to the multi-directional loading *in-vivo*.

Furthermore, previous studies in the literature have been conducted on in-house fixed pericardium [17], [32], [34]–[36], [39]. This study investigated commercially available GLBP, which displayed notable differences to previously reported results. Most importantly, the experiments conducted by Sun et al. [17]**,** which has been employed in a number of computational studies [40]–[42], exhibits a very different stress-strain response to that seen here. Specifically, PD specimens stretched to 16% strain, reached a stress value of 1 MPa. In contrast, the average failure strain of commercial PD specimens was 16% strain in this study; corresponding to a mean stress value of 16.3 MPa (see Figure 4 (c)). A primary difference between such in-house fixed

pericardium and commercially available pericardium is its exposure time to glutaraldehyde. In studies such as Sun et al. [17], the tissue is fixed in glutaraldehyde for a short period of time and then stored in PBS prior to testing. In contrast, commercially fixed tissue is stored in glutaraldehyde until use.

The loading environment employed in this study was simplified in comparison to that of *in-vivo*, where leaflets are subjected to complex, multidirectional loading [6]. Thus, to investigate the response of GLBP under physiological conditions, future experimental set-ups will require incorporation of biaxial and flexural cyclic loading. However, the experiments in the present study do provide an insight into the direct relationship between fibre orientation and loading direction. Various studies in the literature have conducted cyclic testing of GLBP, however these studies did not compare the fatigue performance of specimens of different fibre orientations [17], [22], [43]–[45]. Additionally, the stress-strain curves presented in Figure 4 show that sample groups (XD, HD, PD) behave similarly in the low-strain region, with significant divergences becoming evident as the maximum ultimate tensile strengths are approached. The early failure under cyclic loading seen in XD specimens (Figure 6) may explain premature failures reported clinically [13]–[15].

In conclusion, the results presented in this study illustrate the significant influence of fibre orientation and dispersion on the mechanical performance of GLBP, notably the extremely weak fatigue properties if samples are tested in the XD orientation. Moreover, this indicates that pre-characterisation of leaflet architecture may be a critical factor in future strategies to improve leaflet durability.

5. Acknowledgements

This research is funded by the Irish Research Council and Boston Scientific Corporation ((EBPPG/2016/353).

6. References

[1] V. T. Nkomo, J. M. Gardin, T. N. Skelton, J. S. Gottdiener, C. G. Scott, and M. Enriquez-Sarano, “Burden of valvular heart diseases: a population-based study,” *Lancet*, vol. 368, no. 9540, pp. 1005–1011, Sep. 2006.

[2] A. Carpentier *et al.*, “Reconstructive surgery of mitral valve incompetence: ten-year appraisal.,” *J. Thorac. Cardiovasc. Surg.*, vol. 79, no. 3, pp. 338–48, Mar. 1980.

[3] C. M. Otto, “Timing of aortic valve surgery.,” *Heart*, vol. 84, no. 2, pp. 211–8, Aug. 2000.

[4] S. P. Hoerstrup and B. Weber, “Biological Heart Valves,” *Eur. Heart J.*, vol. 36, no. 6, pp. 325–332, Feb. 2015.

[5] C. Mädler, C. Cardiologist, and S. Lewis, “Anticoagulation in patients with heart valve replacements - Guideline for primary and secondary care,” *Aneurin Bevan University Health Board*. 2015.

[6] M. S. Sacks, W. D. Merryman, and D. E. Schmidt, “On The Biomechanics of Heart Valve Function,” *J. Biomech.*, vol. 42, no. 12, pp. 1804–1824, 2009.

[7] M. Abbasi, M. S. Barakat, K. Vahidkhah, and A. N. Azadani, “Characterization of three-dimensional anisotropic heart valve tissue mechanical properties using inverse finite element analysis,” *J. Mech. Behav. Biomed. Mater.*, vol. 62, pp. 33–44, 2016.

[8] M. S. Sacks and F. J. Schoen, “Collagen fiber disruption occurs independent of calcification in clinically explanted bioprosthetic heart valves,” *J. Biomed.*

Mater. Res., vol. 62, no. 3, pp. 359–371, 2002.

[9] N. Vyavahare *et al.*, “Mechanisms of bioprosthetic heart valve failure: fatigue causes collagen denaturation and glycosaminoglycan loss.,” *J. Biomed. Mater. Res.*, vol. 46, no. 1, pp. 44–50, Jul. 1999.

[10] I. Vesely, “The evolution of bioprosthetic heart valve design and its impact on durability.,” *Cardiovasc. Pathol.*, vol. 12, no. 5, pp. 277–86.

[11] K. Li and W. Sun, “Simulated transcatheter aortic valve deformation: A parametric study on the impact of leaflet geometry on valve peak stress,” *Int. j. numer. method. biomed. eng.*, vol. 33, no. 3, p. e02814, Mar. 2017.

[12] R. F. Siddiqui, J. R. Abraham, and J. Butany, “Bioprosthetic heart valves: modes of failure,” *Histopathology*, vol. 55, no. 2, pp. 135–144, Aug. 2009.

[13] M. Hamamoto, T. Kobayashi, M. Ozawa, and K. Yoshimura, “Pure Cusp Tear of Trifecta Bioprosthesis 2 Years after Aortic Valve Replacement.,” *Ann. Thorac. Cardiovasc. Surg.*, vol. 23, no. 3, pp. 157–160, Jun. 2017.

[14] P. C. Cremer *et al.*, “Early bioprosthetic valve failure: A pictorial review of rare causes,” *JACC Cardiovasc. Imaging*, vol. 8, no. 6, pp. 737–740, 2015.

[15] T. Rodriguez-Gabella, P. Voisine, R. Puri, P. Pibarot, and J. Rodés-Cabau, “Aortic Bioprosthetic Valve Durability: Incidence, Mechanisms, Predictors, and Management of Surgical and Transcatheter Valve Degeneration.,” *J Am Coll Cardiol*, vol. 70, p. 1013–1028., 2017.

[16] P. Aguiari, M. Fiorese, L. Iop, G. Gerosa, and A. Bagno, “Mechanical testing of pericardium for manufacturing prosthetic heart valves,” *Interact. Cardiovasc. Thorac. Surg.*, vol. 22, no. 1, pp. 72–84, Jan. 2016.

[17] W. Sun, M. Sacks, G. Fulchiero, J. Lovekamp, N. Vyavahare, and M. Scott, “Response of heterograft heart valve biomaterials to moderate cyclic loading,” *J. Biomed. Mater. Res.*, vol. 69A, no. 4, pp. 658–669, Jun. 2004.

[18] C. E. Crofts and E. A. Trowbridge, “The tensile strength of natural and chemically modified bovine pericardium,” *J. Biomed. Mater. Res.*, vol. 22, no. 2, pp. 89–98, 1988.

[19] E. A. Trowbridge, M. M. Black, and C. L. Daniel, “The mechanical response of glutaraldehyde-fixed bovine pericardium to uniaxial load,” *J. Mater. Sci.*, vol. 20, no. 1, pp. 114–140, 1985.

[20] D. Chachra, P. F. Gratzer, C. A. Pereira, and J. M. Lee, “Effect of applied uniaxial stress on rate and mechanical effects of cross-linking in tissue-derived biomaterials,” *Biomaterials*, vol. 17, no. 19, pp. 1865–1875, 1996.

[21] A. Mirnajafi, J. Raymer, M. J. Scott, and M. S. Sacks, “The effects of collagen fiber orientation on the flexural properties of pericardial heterograft biomaterials,” *Biomaterials*, vol. 26, no. 7, pp. 795–804, 2005.

[22] T. L. Sellaro, “Effects of Collagen Orientation on the Medium-Term Fatigue Response of Heart Valve Biomaterials,” *Georg. Washingt. Univ.*, pp. 1–93, 2003.

[23] P. Zioupos, J. C. Barbenel, and J. Fisher, “Mechanical and optical anisotropy of bovine pericardium,” *Med. Biol. Eng. Comput.*, vol. 30, no. 1, pp. 76–82, Jan. 1992.

[24] M. S. Sacks, C. J. Chuong, and R. More, “Collagen fiber architecture of bovine pericardium.,” *ASAIO J.*, vol. 40, no. 3, pp. M632-7, 1992.

[25] M. S. Sacks and C. J. Chuong, “Orthotropic Mechanical Properties of Chemically Treated Bovine Pericardium,” *Ann. Biomed. Eng.*, vol. 26, no. 5, pp. 892–902, Sep. 1998.

[26] E. D. Hiester and M. S. Sacks, “Optimal bovine pericardial tissue selection sites. II. Cartographic analysis,” *J. Biomed. Mater. Res.*, vol. 39, no. 2, pp. 215–221, Feb. 1998.

[27] K. L. Billiar and M. S. Sacks, “Biaxial mechanical properties of the natural and glutaraldehyde treated aortic valve cusp--Part II: A structural constitutive model,” *J. Biomech. Eng.*, vol. 122, no. 1, pp. 23–30, 2000.

[28] R. T. Gaul, D. R. Nolan, and C. Lally, “Collagen fibre characterisation in arterial tissue under load using SALS,” *J. Mech. Behav. Biomed. Mater.*, vol. 75, no. July, pp. 359–368, 2017.

[29] M. S. Sacks, D. B. Smith, and E. D. Hiester, “A Small Angle Light Scattering Device for Planar Connective Tissue Microstructural Analysis,” *Ann. Biomed. Eng.*, vol. 25, pp. 678–589, 1997.

[30] D. Haskett, G. Johnson, A. Zhou, U. Utzinger, and J. Vande Geest, “Microstructural and biomechanical alterations of the human aorta as a function of age and location,” *Biomech. Model. Mechanobiol.*, vol. 9, no. 6, pp. 725–736, Dec. 2010.

[31] F. Baaijens, C. Bouten, and N. Driessen, “Modeling collagen remodeling,” *J. Biomech.*, vol. 43, pp. 166–175, 2010.

[32] E. Pasquino, S. Pascale, M. Andreon, S. Rinaldi, F. Laborde, and M. Galloni, “Bovine pericardium for heart valve bioprostheses:in vitro andin vivo characterization of new chemical treatments,” *J. Mater. Sci. Mater. Med.*, vol. 5, no. 12, pp. 850–854, 1994.

[33] A. C. Duncan and D. Boughner, “Effect of dynamic glutaraldehyde fixation on the viscoelastic properties of bovine pericardial tissue,” *Biomaterials*, vol. 19, no. 7–9, pp. 777–783, Apr. 1998.

[34] J. M. García Páez *et al.*, “Mechanical effects of increases in the load applied in uniaxial and biaxial tensile testing: Part I. Calf pericardium,” *J. Mater. Sci. Mater. Med.*, vol. 13, no. 4, pp. 381–388, 2002.

[35] D. Oswal, S. Korossis, S. Mirsadraee, H. Wilcox, J. Fisher, and E. Ingham,

"Biomechanical Characterization of Decellularized and Cross-Linked Bovine Pericardium," *J Hear. Valve Dis*, vol. 16, no. 2, 2007.

[36] F. M. Sánchez-Arévalo, M. Farfán, D. Covarrubias, R. Zenit, and G. Pulos, "The micromechanical behavior of lyophilized glutaraldehyde-treated bovine pericardium under uniaxial tension," *J. Mech. Behav. Biomed. Mater.*, vol. 3, no. 8, pp. 640–646, 2010.

[37] R. Gauvin *et al.*, "A comparative study of bovine and porcine pericardium to highlight their potential advantages to manufacture percutaneous cardiovascular implants," *J. Biomater. Appl.*, vol. 28, no. 4, pp. 552–565, 2013.

[38] J. Hülsmann *et al.*, "Transplantation material bovine pericardium: Biomechanical and immunogenic characteristics after decellularization vs. glutaraldehyde-fixing," *Xenotransplantation*, vol. 19, no. 5, pp. 286–297, 2012.

[39] A. Caballero, F. Sulejmani, C. Martin, T. Pham, and W. Sun, "Evaluation of transcatheter heart valve biomaterials: Biomechanical characterization of bovine and porcine pericardium," *J. Mech. Behav. Biomed. Mater.*, vol. 75, pp. 486–494, 2017.

[40] C. Martin and W. Sun, "Modeling of Tissue Fatigue Damage in Bio-Prosthetic Heart Valve," in *ASME 2011 Summer Bioengineering Conference, Parts A and B*, 2011, p. 1217.

[41] M. S. Sacks, W. Zhang, and S. Wognum, "A novel fibre-ensemble level constitutive model for exogenous cross-linked collagenous tissues," *Interface Focus*, vol. 6, no. 1, p. 20150090, 2015.

[42] D. C. Gloeckner, K. L. Bilhar, and M. A. Sacks, "Effects of Mechanical Fatigue on the Bending Properties of Porcine Bioprosthetic Heart Valve," *ASAIO J.*, pp. 59–63, 1999.

[43] T. L. Sellaro, D. Hildebrand, Q. Lu, N. Vyavahare, M. Scott, and M. S. Sacks,

"Effects of collagen fiber orientation on the response of biologically derived soft tissue biomaterials to cyclic loading," *J. Biomed. Mater. Res. Part A*, vol. 80A, no. 1, pp. 194–205, Jan. 2007.

[44] D. Mavrilas, E. A. Sinouris, D. H. Vynios, and N. Papageorgakopoulou, "Dynamic mechanical characteristics of intact and structurally modified bovine pericardial tissues," *J. Biomech.*, vol. 38, no. 4, pp. 761–768, 2005.

[45] A. Mirnajafi, B. Zubiate, and M. S. Sacks, "Effects of cyclic flexural fatigue on porcine bioprosthetic heart valve heterograft biomaterials," *J. Biomed. Mater. Res. Part A*, vol. 94A, no. 1, pp. 205–213, Jul. 2010.

Appendix A

Table 1: *Specimen Summary- Monotonic Testing*

Sample	Mean Angle (°)	Eccentricity	UTS (MPa)	Stiffness (MPa)	Failure Strain (%)
PD 1	-2.56	0.7183	24.92	160.23	19.79
PD 2	-5.33	0.726	15.71	184.38	12.71
PD 3	1.43	0.724	21.87	167.17	17.08
PD 4	2.145	0.726	8.26	94.60	11.15
PD 5	-4.29	0.733	13.18	136.19	13.18
PD 6	-6.875	0.74	13.88	126.81	13.40
XD 1	79.33	0.7763	1.11	16.68	5.34
XD 2	75	0.7455	5.94	41.51	12.24
XD 3	81.375	0.718	0.03	0.68	1.71
XD 4	80.02	0.722	7.96	4.24	12.34
XD 5	87.04	0.705	2.48	43.52	12.72

XD 6	84	0.7236	5.85	50.49	13.12
HD 1	N/A	0.58	17.85	103.97	15.20
HD 2	N/A	0.52	10.93	81.58	13.10
HD 3	N/A	0.56	17.83	95.56	15.45
HD 4	N/A	0.47	11.17	81.88	13.70
HD 5	N/A	0.54	7.81	73.56	10.70
HD 6	N/A	0.629	10.20	68.6	14.04

Table 2: *Specimen Summary- Cyclic Testing*

Sample	**Mean Angle**	**Eccentricity**	**Cycles to Failure**	**Initial Stiffness (MPa)**	**Final Stiffness (MPa)**
PD 1	-22.042	0.70	N/A	141.29	150.96
PD 2	6.58	0.69	N/A	160.54	176.04
PD 3	0	0.73	N/A	194.93	250.81
PD 4	34.1	0.712	N/A	148.41	187.22
PD 5	-31.125	0.763	N/A	181.65	224.06
PD 6	-33.6	0.769	N/A	162.32	181.00
XD 1	93	0.8	1	50.48	40.77
XD 2	67	0.69	2	25.85	25.09
XD 3	98	0.68	10	93.82	91.69
XD 4	121	0.73	23	70.18	58.07
XD 5	76	0.68	45 561	39.41	N/A
XD 6	78	0.65	N/A (run-out)	70.722	44.21